AGU PUBLICATIONS

JGR

Journal of Geophysical Research: Atmospheres

RESEARCH ARTICLE
10.1002/2015JD024101

Key Points:
- A second harmonic term (2 cycles/yr) is identified as a ubiquitous feature of ozone in the MBL
- Quantitative metrics are provided to serve as the basis for future model-measurement comparisons
- The treatment of MBL dynamics in CCMs is not adequate to reproduce the isolation of the MBL

Correspondence to:
D. D. Parrish,
David.D.Parrish@noaa.gov

Citation:
Parrish, D. D., et al. (2016), Seasonal cycles of O_3 in the marine boundary layer: Observation and model simulation comparisons, *J. Geophys. Res. Atmos.*, *121*, 538–557, doi:10.1002/2015JD024101.

Received 17 AUG 2015
Accepted 11 DEC 2015
Accepted article online 17 DEC 2015
Published online 14 JAN 2016

Seasonal cycles of O_3 in the marine boundary layer: Observation and model simulation comparisons

D. D. Parrish[1,2], I. E. Galbally[3], J.-F. Lamarque[4], V. Naik[5], L. Horowitz[6], D. T. Shindell[7], S. J. Oltmans[2,8], R. Derwent[9], H. Tanimoto[10], C. Labuschagne[11], and M. Cupeiro[12]

[1]NOAA ESRL Chemical Sciences Division, Boulder, Colorado, USA, [2]CIRES, University of Colorado Boulder, Boulder, Colorado, USA, [3]CSIRO Oceans and Atmosphere, PMB1, Aspendale, Victoria, Australia, [4]National Center for Atmospheric Research, Boulder, Colorado, USA, [5]UCAR/NOAA Geophysical Fluid Dynamics Laboratory, Princeton, New Jersey, USA, [6]NOAA Geophysical Fluid Dynamics Laboratory, Princeton, New Jersey, USA, [7]Nicholas School of the Environment, Duke University, Durham, North Carolina, USA, [8]NOAA ESRL Global Monitoring Division, Boulder, Colorado, USA, [9]rdscientific, Newbury, UK, [10]National Institute for Environmental Studies, Tsukuba, Japan, [11]South African Weather Service, Stellenbosch, South Africa, [12]Estación GAW Ushuaia, Servicio Meteorológico Nacional, Ushuaia, Argentina

Abstract We present a two-step approach for quantitatively comparing modeled and measured seasonal cycles of O_3: (1) fitting sine functions to monthly averaged measurements and model results (i.e., deriving a Fourier series expansion of these results) and (2) comparing the phase and amplitude of the statistically significant terms between the models and measurements. Two and only two sine terms are sufficient to quantify the O_3 seasonal cycle in the marine boundary layer (MBL) in both the measurements and the model results. In addition to the expected fundamental (one sine cycle per year), a second harmonic term (i.e., two sine cycles per year) is identified as a ubiquitous feature of O_3 in the MBL. Three chemistry climate models (Community Atmosphere Model with chemistry, GFDL-CM3, and GISS-E2-R) approximately reproduce many features of the measured seasonal cycles at MBL surface sites throughout the globe, with some notable quantitative disagreements, but give divergent results that do not agree with O_3 sonde measurements above the MBL. This disagreement and divergence of results between models indicate that the treatment of the MBL dynamics in the chemistry-climate models is not adequate to reproduce the isolation of the MBL indicated by the observations. Within the MBL the models more accurately reproduce the second harmonic term than the fundamental term. We attribute the second harmonic term to the second harmonic of opposite phase in the photolysis rate of O_3, while the fundamental term evidently has many influences. The parameters derived from the Fourier series expansion of the measurements are quantitative metrics that can serve as the basis for future model-measurement comparisons.

1. Introduction

Ozone (O_3) is central to troposphere chemistry where it is primarily of secondary origin, produced through photochemical oxidation of methane, carbon monoxide, and nonmethane volatile organic compounds in the presence of nitrogen oxides. Downward transport from the stratosphere is an additional significant source. Photolysis of O_3 is the primary source of hydroxyl radicals, which are the major initiator of the photochemical oxidation cycles of the troposphere [*Levy*, 1971]. Ozone is an important component of photochemical air pollution, with enhanced concentrations in surface air causing negative impacts on human health, agricultural and forest yields, and natural ecosystems [e.g., *Royal Society*, 2008]. Tropospheric O_3 is also an important greenhouse gas, since its long-term concentration changes have increased the radiative forcing of climate.

Chemistry-climate models (CCMs; e.g., the models included in the Atmospheric Chemistry and Climate Model Intercomparison Project [*Lamarque et al.*, 2013]) are the tools we rely on to provide estimates of the radiative forcing of tropospheric O_3, as they can calculate the changes of O_3 concentrations from the preindustrial period to the present and project these changes into the future [e.g., *Stevenson et al.*, 2013]. These same or closely related chemical transport models (CTMs), are utilized to calculate background O_3 concentrations [*Fiore et al.*, 2014; *Zhang et al.*, 2014] transported into regions where air quality concerns require such calculations to set achievable air quality standards. Building confidence in the simulations of O_3 concentrations and their long-term changes by these complex models requires thorough evaluation against observations [*Parrish et al.*, 2014; *Cooper et al.*, 2014; *Brown-Steiner et al.*, 2015; *Schnell et al.*, 2015]. Quantitative comparisons of model calculations with measurements have indicated that at least three example CCMs poorly reproduce

observed long-term O_3 changes [*Parrish et al*., 2014]. For example, over Europe (where the longest, high-quality O_3 records have been collected) the models capture only about one half of observed changes and little of the observed seasonal differences in the changes. However, no diagnostic of the cause of the model shortcomings has been provided by this analysis beyond raising the obvious issue of emission uncertainties. Describing an approach to model-measurement comparisons that provides some diagnostics that can lead to model improvement is one goal of this work.

In this paper we address a question that provides a process-based evaluation of models: Can CCMs accurately reproduce the tropospheric O_3 seasonal cycle observed at a variety of approximately baseline, marine boundary layer (MBL) sites throughout the globe? Our hypothesis is that models must realistically treat many of the O_3 production, loss, and transport processes to accurately reproduce the seasonal cycle and that disagreement of model results with measurements may provide some information regarding how a given model can be improved. We chose to focus on the MBL because in most regions it receives relatively small anthropogenic emissions and is relatively isolated from the rest of the troposphere, so the multitude of processes that affect tropospheric O_3 concentrations may be simpler in this environment. Further, marine environments lie upwind from North America and Europe; transport from this environment provides the background O_3 concentrations to which anthropogenic enhancements are added. As these anthropogenic enhancements are controlled through air quality improvement programs and ambient concentration standards are tightened, it is becoming increasingly important to accurately quantify the background O_3 concentrations and apportion their sources [e.g., *Cooper et al*., 2015]. CTMs, closely related to CCMs but based upon assimilated or modeled actual meteorology, provide our primary tool for this quantification and source apportionment. Assessing how well these models reproduce the MBL O_3 seasonal cycle throughout the globe is one test of their ability to accurately reproduce the tropospheric O_3 distribution in space and time. Here we compare CCM model results with O_3 measurements from eight MBL data sets. The CCM results considered here are not based on assimilated meteorology, and thus cannot be expected to accurately reproduce seasonal variations in particular years; consequently, multiannual statistical evaluation metrics are required, and that is the approach taken here. The comparison methods developed can also be used for assessment of CTMs, but that is not attempted in this paper. The comparison data sets are selected for (1) minimal impact from local sources and surface deposition removal processes, (2) long-term, high-quality measurement records, and (3) absence of influence of wintertime O_3 destruction through bromine chemistry [e.g., *Oltmans et al*., 1989]. The chemistry of the wintertime O_3 destruction is not included in the CCMs yet can strongly affect the O_3 seasonal cycle at some arctic sites.

2. Observations and Model Simulations

Here we give only very brief overviews of the observations and model results compared in this paper. We limit our quantitative comparisons to observational data sets from three of the northern midlatitude MBL data sets (Mace Head, Pacific MBL, and Japanese MBL) examined by *Parrish et al*. [2014], plus five additional sites, including one at northern midlatitudes (Storhofdi and Iceland), three from the southern midlatitudes (Ushuaia, Argentina; Cape Grim, Australia; and Cape Point, South Africa), and a tropical site (Samoa). Measurements from three additional sites (Arrival Heights, Antarctica; Ragged Point, Barbados; and Tudor Hill, Bermuda) are included to provide comparisons and contrasts with the other measurement data sets. Table 1 gives some information regarding the sites including the dates of available data; all sites are chosen to represent baseline O_3 (here understood as representative of continental to hemispheric scales) over the longest available time spans. The mean monthly O_3 concentrations for the three northern midlatitude sites discussed by *Parrish et al*. [2014] are derived from archived data sets as described by *Parrish et al*. [2013]. Monthly mean data for Samoa, Iceland, Bermuda, Barbados, and Antarctica were calculated from hourly data archived at NOAA/GMD (http://www.esrl.noaa.gov/gmd/dv/ftpdata.html). Most of the ozone records used in this work are also available from the WMO Global Atmosphere Watch World Data Centre for Greenhouse Gases. Ozone concentrations are consistently expressed as mole fractions (i.e., mixing ratios) in units of nmol O_3/mole air, referred to as ppb throughout the paper.

The monthly mean data represent means over the full 24 h period. However, three of the measurement data sets have been filtered for baseline conditions. At Cape Point, O_3 data collected through an inlet 30 m above the ground were filtered according to wind direction. The Mace Head and the U.S. Pacific MBL data were

Table 1. MBL Surface Data Sets Analyzed

Monitoring Site	Dates	Latitude/Longitude
Arrival Heights, Antarctica	1997–2013	77°50′S/166°12′E
Ushuaia, Argentina	1994–2013	54°50′S/68°18′W
Cape Grim, Australia	1982–2010	40°41′S/144°41′E
Cape Point, South Africa	1983–2011	34°21′S/18°29′E
Cape Matatula, Samoa	1976–2010	14°14′S/170°34′W
Ragged Point, Barbados	1989–2010[b]	13°10′N/59°26′W
Tudor Hill, Bermuda	1988–2010[b]	32°16′N/64°53′W
Japanese MBL[a]	1998–2011	38°15′N/138°24′E
Pacific MBL, United States[a]	1990–2010	41°3′N/124°9′W
Mace Head, Ireland	1989–2014	53°10′N/9°30′W
Storhofdi, Iceland	1992–2010	63°20′N/20°17′W

[a]Data sets combining measurements from multiple sites. Latitude/Longitude is for sites at Sado Island, Japan, and Trinidad Head, United States.
[b]Data sets with large gap in observations: Barbados (1995–2005) and Bermuda (1999–2002).

filtered according to trajectory analysis and measured winds, respectively; *Parrish et al*. [2013] give details. A recent update to the Mace Head data including results through 2014 has recently been provided by a coauthor (R. D.); these data are analyzed here. No filtering has been performed on measurements from the other sites or the model results for any of the sites.

The model calculations are identical to those examined by *Parrish et al*. [2014], who give short model descriptions with references to more complete descriptions. These simulations were contributed to the Coupled Model Intercomparison Project Phase 5, and are well documented; *Eyring et al*. [2013] present a table summarizing the models, and *Lamarque et al*. [2013] describe the models in detail. The analyses included here are based on modeled monthly mean O_3 concentrations including all times of day at the longitude, latitude, and altitude of each observation site. Calculations from three global chemical climate models are examined: the Community Atmosphere Model expanded to include interactive chemistry (CAM-chem) [*Lamarque et al*., 2010, 2012], the GFDL-CM3 coupled atmosphere-ocean-land-ice model with interactive tropospheric and stratospheric chemistry [*Donner et al*., 2011; *Griffies et al*., 2011], and the GISS-E2-R model [*Shindell et al*., 2013]. For the MBL the lowest model layer is generally evaluated; the thickness of this level was ~150 m, ~60 m, and ~200 m in the CAM-chem, GFDL, and GISS models, respectively. The CAM-chem, GFDL-CM3, and GISS-E2-R models reported results before the beginning of the measurements at any of the sites and continuing through 2009, 2005, and 2011, respectively. The CAM-chem model was run at NCAR, and the model results will be labeled as NCAR throughout the paper.

The seasonal cycles are generally calculated from the entire measurement data set. One exception is the Ushuaia data set, where April through August 1999 are excluded since those data report much lower concentrations than seen in those seasons in any other years of measurements, although the reason for these low concentrations is unknown. We also note that the Pacific MBL and the Japan MBL data sets combine data from five and three separate sites, respectively, as discussed by *Parrish et al*. [2014]; from 1995 through 2001 summer baseline data are not available for the Pacific MBL as discussed by *Parrish et al*. [2009]. The software used to calculate the Fourier transforms requires complete years of data; in any year with data missing in one or more months, the complete year of data was removed from these calculations.

The seasonal cycles are generally calculated for the model results from the beginning of the measurements through the end of the modeling period. However, for the measurements that begin in 1989 or later, two earlier years of the GFDL model results (which end in 2005) are included to give a more nearly similar time period for the measurements and model results. Additionally, model results included for the Samoa calculations begin in 1976 (1974 for the GFDL model) to improve the precision of the seasonal cycle determination at this tropical site, which is characterized by very low O_3 concentrations. Finally, the NCAR model did not report results for December 2009; to complete the Fourier transform calculations, December 2008 model results were duplicated to complete year 2009 for these calculations only.

3. Analysis

Our goal is to derive a quantitative description of the seasonal cycle of tropospheric O_3 from both observations and model results. To simplify model-measurement comparisons this quantitative description is selected so that only a small number of statistically significant parameters are required for its definition. These parameters serve as quantitative metrics for the present comparisons; those derived from the measurements can also serve as metrics to which results from other model calculations can be compared. Derivation of these defining parameters involves three steps for both the data and model results: (1) detrending (i.e., removing any systematic

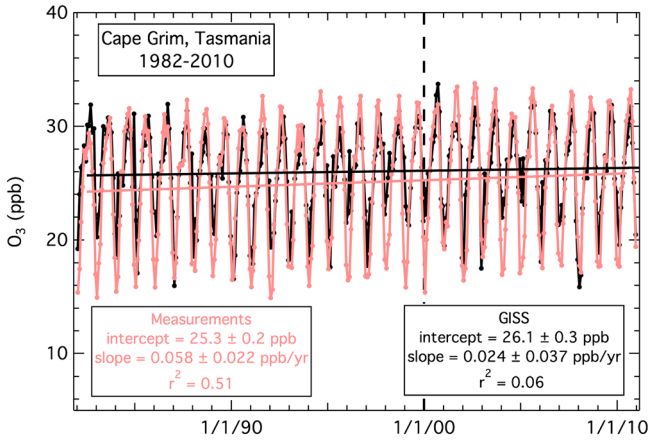

Figure 1. Time series of monthly average O_3 mixing ratios measured at Cape Grim and modeled by the GISS CCM. The lines show linear regression fits to annual average data. Long-term changes are removed (i.e., detrended) by subtracting the linear regression fits and then adding a term to preserve the average of the original data set. The parameters of the linear fits with 95% confidence limits are annotated. The intercepts are at year 2000 as indicated by dashed vertical line.

and long term-change), (2) performing a Fourier transform to determine the number of harmonic terms necessary to define the respective seasonal cycles, and (3) fitting sine functions to these harmonic terms using least squares regression analysis. Defining each sine function requires two parameters, the amplitude, A, and a phase angle, ϕ. As we will show, two and only two sine functions are unambiguously statistically justified in the seasonal cycles considered here. Thus, the four parameters of the two sine functions, plus Y_0, the annual average O_3 concentration over the entire set of observations or model results, constitute the five comparison metrics we will use.

In all cases we analyze monthly mean data and model results. The seasonal cycle derived from monthly means is indistinguishable from those derived from higher-frequency data, but monthly means provide no sensitivity to higher-frequency variability such as synoptic and diurnal variations. In effect, working with monthly means imposes a low-pass filter on the analysis, but this filter does not affect quantification of the seasonal cycle.

The detrending process is based upon linear (or for one site quadratic) regression analysis of the annual mean data and model results. The detrending process is accomplished by subtracting from each monthly mean the interpolated regression fit to the annual means. Then the average of all detrended monthly means (which is close to zero) is subtracted from each monthly mean, and the average of the entire original, undetrended data is added. The result of this process is a set of monthly mean data with no long-term trend and with the average of the original data set preserved.

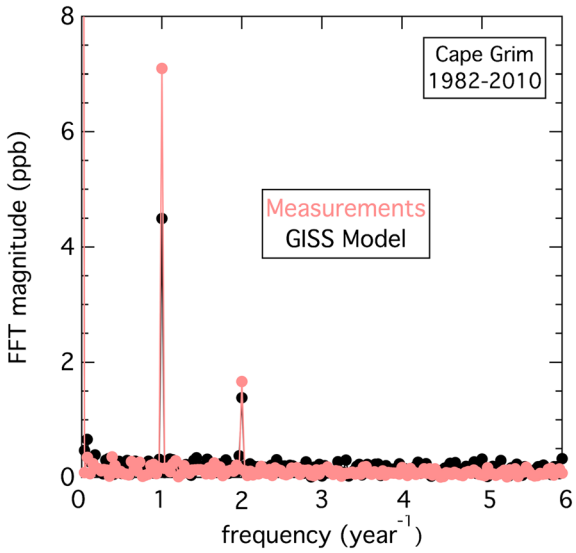

Figure 2. Results of Fourier transform of the data and model results shown in Figure 1. The only significant contributions to the seasonal cycle are the fundamental and the second harmonic, i.e., one and two sine cycles per year.

Figure 1 illustrates the linear regressions for the measurements and results from one CCM at Cape Grim, an example site located in the Southern Hemisphere, with the regression parameters (slope and year 2000 intercept) annotated. At many sites, statistically significant slopes indicating significant long-term trends are determined for both measurement and model results. *Parrish et al.* [2014] show that there is significant disagreement in the trends between models and measurements at northern midlatitudes. *Cooper et al.* [2014] discuss the measured and modeled trends for 9 of the 11 data sets considered here. Measurements and models agree that trends are much smaller at the Southern Hemisphere and tropical sites than at northern midlatitudes. Most of the measured and modeled

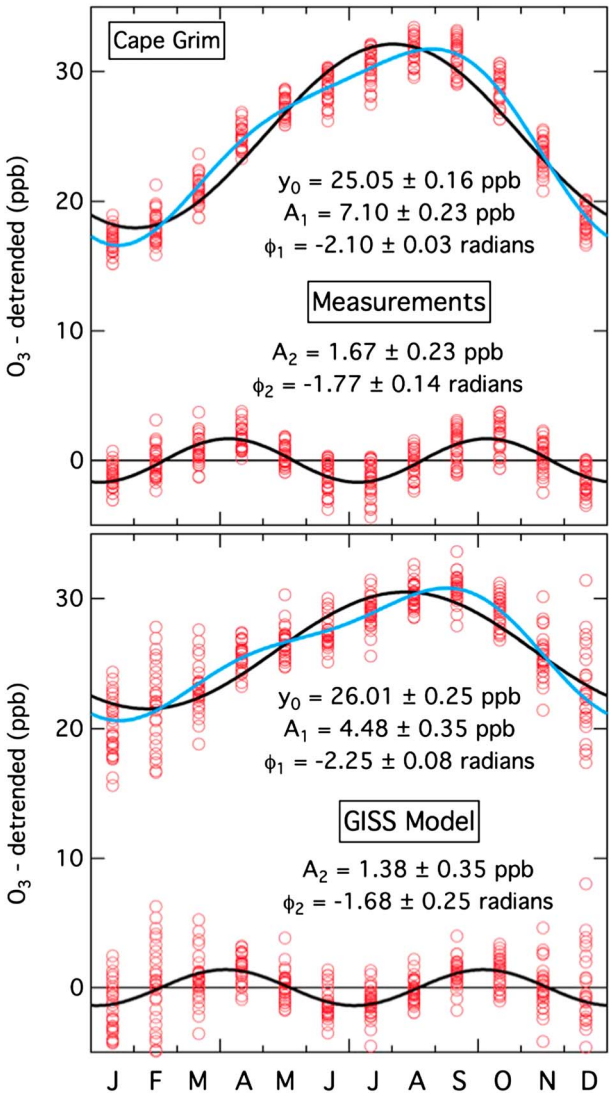

Figure 3. Sine function fits to the data and model results of Figure 1, after detrending (see text and Figure 1 caption). The black curves give the least squares regressions to the fundamental and second harmonic terms, and the blue curves show their sums. The data points about the *x* axis are the residuals between the measurements and the fundamental fit. The fit parameters with 95% confidence limits are annotated.

trends in the Southern Hemisphere agree within their confidence limits, although there are some statistically significant disagreements. Most notably, the GFDL model finds small negative trends in the Southern Hemisphere, while the other two models and the measurements find small positive trends. The detrending process was based on linear fits to the annual mean data for all measurement and model results, except for the measurements at Mace Head. At only this site was the second-order term considered to be unambiguously statistically significant; see *Parrish et al.* [2014] for additional discussion of regression fits of second and higher order. As can be seen from the example illustrated in Figure 1, the variability of the monthly means is much larger than the variability associated with the long-term trend, so the derived seasonal cycles depend only weakly on the details of the detrending process.

Performing a Fourier transform of the detrended monthly averages is a convenient means to identify the harmonics with the largest contributions to the seasonal cycle. Figure 2 shows the results of the Fourier transform of the data and model results of Figure 1 after the detrending process. It is clear that two and only two harmonic terms make significant contributions. There is also a term at zero frequency (off scale in Figure 2) that corresponds to the annual average concentration. Interestingly, at each of the eight sites the Fourier transforms of the measurements and the results of all three models give the same result; two and only two harmonic terms have magnitudes that are well above the noise. These terms have one sine cycle per year (the fundamental) and two sine cycles per year (the second harmonic). *Fabian and Pruchniewicz* [1977] performed a similar Fourier analysis of O_3 seasonal cycles; however, they analyzed data sets of only a very few years in length and found that only the fundamental term was significant.

Least squares regression fits of sine functions (i.e., equation (1)) to detrended monthly mean O_3 concentrations and model results (e.g., Figure 1) allow the parameters defining the fundamental and second harmonic terms to be derived:

$$y = Y_o + A_1 * \sin(\chi + \phi_1) + A_2 * \sin(2 * \chi + \phi_2). \quad (1)$$

These five parameters are discussed above; the variable χ spans 1 year's time period in radians from 0 to 2π. The second and third terms in equation (1) are the fundamental and second harmonic. Figure 3 illustrates the

Table 2. Parameters of Fourier Series Fits to O_3 Seasonal Cycles for the 11 MBL Surface Data Sets Listed in Table 1

Monitoring Site	Y_o[a] (ppb)	A_1 (ppb)	ϕ_1 (rad)	A_2 (ppb)	ϕ_2 (rad)	RMSD (ppb)
Arrival Heights, Antarctica	25.7 ± 0.5	9.4 ± 0.8	−1.93 ± 0.08	0.9 ± 0.8	−2.10 ± 0.89	1.5
Ushuaia, Argentina	23.7 ± 0.4	9.0 ± 0.5	−1.97 ± 0.06	1.1 ± 0.5	−2.08 ± 0.47	1.3
Cape Grim, Australia	25.0 ± 0.2	7.1 ± 0.2	−2.10 ± 0.03	1.7 ± 0.2	−1.77 ± 0.14	1.1
Cape Point, South Africa	23.1 ± 0.4	7.2 ± 0.6	−2.09 ± 0.08	0.9 ± 0.6	−2.07 ± 0.60	1.5
Cape Matatula, Samoa	13.5 ± 0.3	5.4 ± 0.4	−2.31 ± 0.08	1.0 ± 0.4	1.59 ± 0.41	2.4
Ragged Point, Barbados	21.2 ± 1.2	5.3 ± 1.7	0.91 ± 0.32	1.1 ± 1.7	1.35 ± 1.55	2.6
Tudor Hill, Bermuda	37.3 ± 1.3	10.3 ± 1.9	0.67 ± 0.18	5.3 ± 1.9	−2.32 ± 0.36	4.4
Japanese MBL	45.1 ± 1.4	8.3 ± 2.0	−0.04 ± 0.24	5.9 ± 2.0	−2.31 ± 0.34	3.4
Pacific MBL, USA	32.0 ± 0.7	5.7 ± 0.9	0.48 ± 0.16	3.5 ± 0.9	−2.30 ± 0.26	3.2
Mace Head, Ireland	38.8 ± 0.4	5.6 ± 0.6	0.50 ± 0.10	3.0 ± 0.6	−2.34 ± 0.20	2.5
Storhofdi, Iceland	38.5 ± 0.5	6.2 ± 0.7	0.53 ± 0.12	3.2 ± 0.7	−2.24 ± 0.23	2.1

[a] Y_o represents the annual average O_3 concentration evaluated over the complete period covered by the measurements.

fitting procedure for the data and model results of Figure 1 with the respective five derived parameters with confidence limits annotated. In each panel the upper black curve is the fundamental fit to the detrended monthly means. The residuals between the monthly means and the fundamental fit are plotted about the axis near the bottom of each panel (red circles). The second harmonic is compared to these residuals as indicated by the lower black curve in each panel. The blue curve in each panel of Figure 3 is the sum of the fundamental and second harmonic terms. This sum is our best estimate of the seasonal cycle derived from the measurements and the model results. Importantly, the five parameters that define this sum represent all of the statistically significant information available regarding the average seasonal cycle in the measurements and model results; these five parameters are the metrics upon which the following model-measurement comparisons are based. Table 2 lists the parameters (with their 95% confidence limits) derived from the regression analysis of the 11 MBL measurement records given in Table 1. We note that there is ambiguity in how the parameters are defined; the convention adopted here is amplitudes > 0 and phase angles as $-\pi < \phi \leq +\pi$.

As expected, the magnitude of Y_o and the amplitudes of the two harmonic terms derived from the regression fit to equation (1) shown in Figure 3 are equal to the magnitudes of those two terms in the respective Fourier transform illustrated in Figure 2. The phase angles of the two harmonic terms can also be derived from Fourier analysis. The regression fits are included here to provide quantitative confidence limits for the five parameters, to allow inclusion of all monthly measured monthly means in the regression fit (the fast Fourier transform software package that we use requires complete years of monthly means), and to give clear illustrations of the fits (i.e., Figure 3).

Fits to higher-order harmonics were investigated; two and only two harmonic terms were unambiguously statistically significant. Small additional contributions from a third harmonic (three sine cycles per year) were infrequently seen. These additional contributions were never larger than half of the second harmonic contribution, and limited to measurements at 1 of the 11 sites listed in Table 1, and to four of the 33 sets of model results considered. The statistical significance of each of these third harmonic contributions is marginal; they will not be considered further.

It is noteworthy that the two sine terms in equation (1) are orthogonal functions, so the information in the data set that defines one term is independent of the information defining the other. Consequently, the derived regression parameters are independent of whether the regression procedure treats each term separately or both terms simultaneously. However, the confidence limits derived for the parameters do vary, and the smallest (i.e., best) confidence limits are derived from a regression procedure that simultaneously derives both terms. All the regressions presented in this work simultaneously treated both terms, and the confidence limits were initially derived assuming that each monthly mean was an independent result, with no autocorrelation in either the measurements or model results. This assumption was checked through autocorrelation analysis, which indicated little or no significant autocorrelation in either the measurements or model results. In the few cases where significant autocorrelation was found, the confidence limits were increased in accord with the indicated number of degrees of freedom in the data, following the procedure suggested by *Leith* [1973]. The resulting 95% confidence limits are included in Table 2.

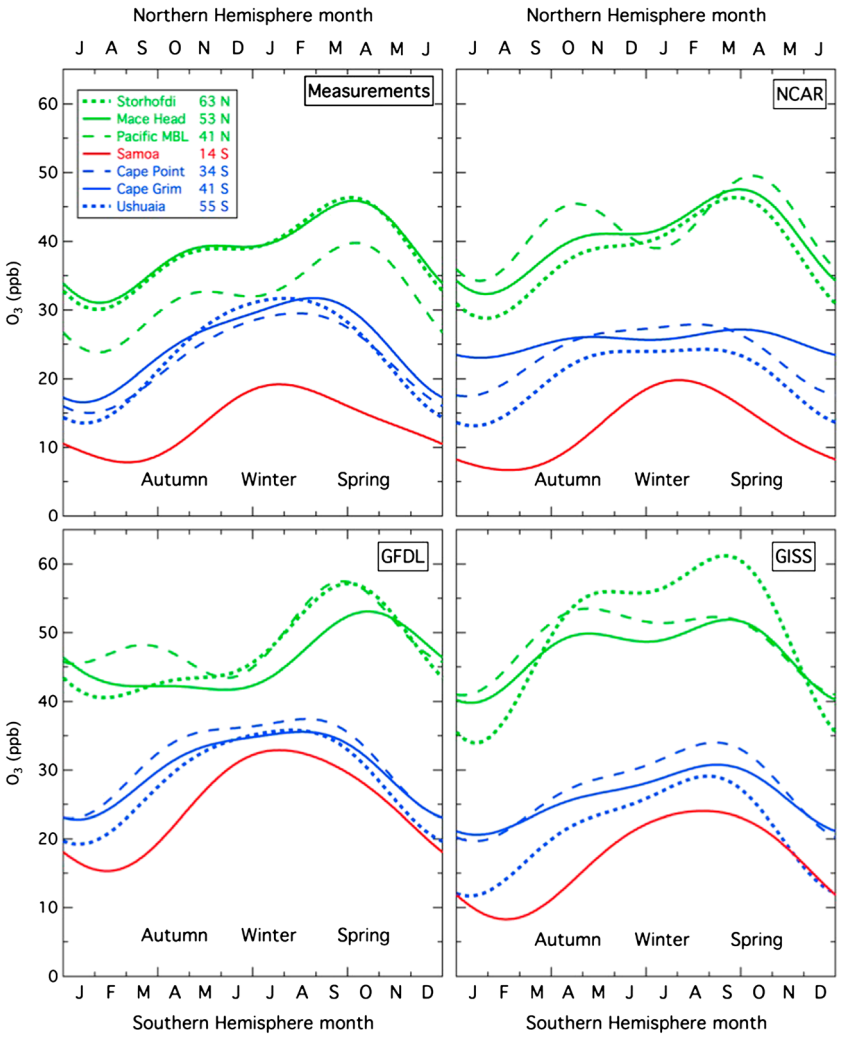

Figure 4. Sum of fundamental and second harmonic fits to measured and modeled seasonal cycles of O_3 mixing ratios at seven marine boundary layer sites. Curves are analogous to the blue curves in Figure 3. Data from the two hemispheres are plotted on *x* axes that locate winter near the center of the graph.

4. Results

4.1. Conceptual Model of the MBL O_3 Seasonal Cycle

The seasonal cycles of O_3 at seven baseline MBL sites as represented by the sum of the fundamental and second harmonic fits are illustrated for measurements and models in Figure 4. Here the Southern Hemisphere results are plotted on the bottom abscissa and those from the Northern Hemisphere on the top abscissa so that winter is near the center of the plot for both hemispheres. The measurements at all sites (Figure 4, top left) show a great deal of similarity. O_3 maximizes in late winter to early spring. The seasonal cycles are particularly uniform at the three southern midlatitude sites. (In this and other figures, northern midlatitude, tropical, and southern extratropical sites are indicated by the colors green, red and blue, respectively). There is a clear systematic latitudinal variation; the overall concentrations at northern midlatitudes are larger than those at southern midlatitudes with the one tropical site exhibiting considerably smaller concentrations. The northern midlatitude sites show more evidence for a double peak in the seasonal cycle, with a secondary maximum in late autumn; as we will discuss, this behavior is due to larger contributions of the second harmonic term at those sites. Each of the three models reproduces many characteristics of the seasonal cycles, but there are clear quantitative differences.

The late winter to early spring maximum and the corresponding late summer minimum is generally interpreted to indicate that the O_3 seasonal cycle in the MBL is dominated by net photochemical destruction of O_3

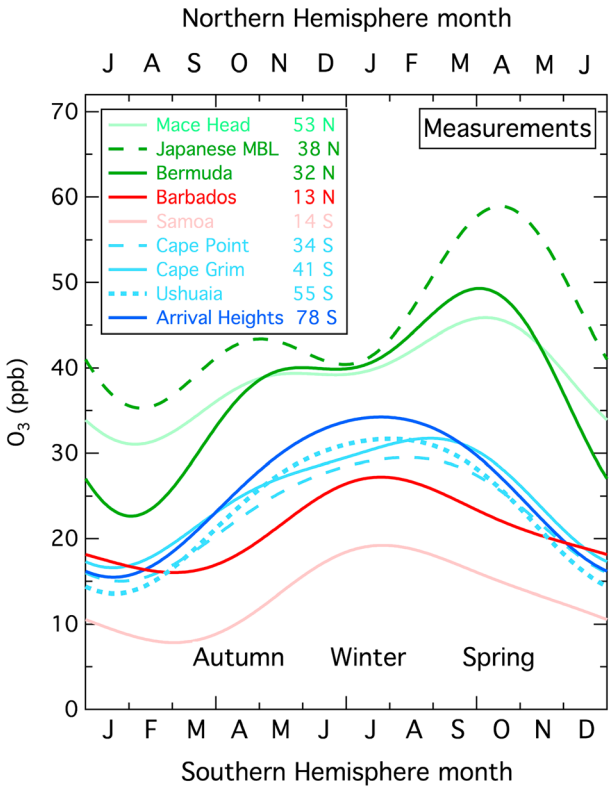

Figure 5. Comparison of seasonal cycles of O_3 mixing ratios at four additional marine boundary sites (dark colors) compared to five of the sites included in Figure 4 (light colors). Figure is in the same as format as Figure 4.

[e.g., *Ayers et al.*, 1992; *Oltmans and Levy*, 1992, 1994], which is expected given the generally small emissions of O_3 precursors within the MBL. To a first approximation, O_3 produced elsewhere is entrained from the free troposphere (FT) into the MBL where it is destroyed through R1–R4.

$$O_3 + h\nu \rightarrow O_2 + O(^1D) \quad \text{(R1)}$$

$$O(^1D) + H_2O \rightarrow 2OH \quad \text{(R2)}$$

$$OH + O_3 \rightarrow O_2 + HO_2 \quad \text{(R3)}$$

$$HO_2 + O_3 \rightarrow OH + 2O_2 \quad \text{(R4)}$$

The O_3 concentration in the MBL reflects the balance between this entrainment and photochemical destruction within the MBL, facilitated by the higher water vapor there. Faster destruction in summer than in winter accounts for the summertime minimum and wintertime maximum. The rate of the destruction processes is directly related to the photolysis rate of O_3 to produce oxygen atoms in the ^1D excited state, $j(O^1D)$, and to the ambient water vapor concentration. Depending on humidity and atmospheric pressure, approximately 10% of the O^1D atoms react with water vapor, providing a net sink of O_3, while the majority is collisionally quenched to the ground state to reform O_3. Hydroxyl radicals produced in R2 initiate reaction sequences that destroy additional O_3 in such pristine environments (R3 and R4). The dominant role of photochemical destruction of O_3 is further evidenced by the diurnal cycles of O_3 at the most pristine locations in the MBL; they generally show maxima near dawn, decreases during the day to minima near sunset followed by increases during nighttime [*Ayers et al.*, 1992; *Oltmans and Levy*, 1994].

The seasonal cycles from four additional sites are shown in Figure 5 and compared to some of the seasonal cycles from Figure 4. (Quantitative model-measurement comparisons are discussed in section 4.2.) Model results have not been obtained for three sites (Bermuda, Barbados, and Arrival Heights) and unambiguous model-measurement comparisons are not possible at the Japanese MBL sites as discussed in section 4.4.2 below. The results in Figure 5 emphasize the applicability of the conceptual model of the MBL O_3 seasonal cycles. Bermuda is similar to Mace Head with a deeper summertime minimum, reflecting its location closer to the equator and its greater summertime isolation from continental O_3 sources, and a higher early springtime maximum when Bermuda receives continental outflow from North America carrying O_3 photochemically produced from anthropogenic sources [*Oltmans and Levy*, 1994]. The Japanese MBL experiences the highest ozone concentrations, presumably because it receives pollution outflow from the Asian continent. Barbados is a tropical site in the Northern Hemisphere that is approximately the same distance from the equator as is Samoa in the Southern Hemisphere. The seasonal cycle is nearly identical at these two tropical sites, although the absolute concentrations are about 8 ppb higher at the Northern Hemisphere Barbados site throughout the year; the parameters of the fundamental and second harmonic terms at these two tropical sites (Table 2) all agree within their confidence limits, except the fundamental is 3.2 ± 0.3 rad (6.1 ± 0.6 months) out of phase as expected for the different hemispheres. The seasonal cycle at the Arrival Heights site in Antarctica is similar to those at the southern midlatitude sites, except the wintertime maximum is somewhat larger. We cursorily investigated several additional northern midlatitude MBL sites (Westerland and Zingst, Germany; Kollumerwaard, Netherlands; Monte Velho, Portugal; and Sable Island,

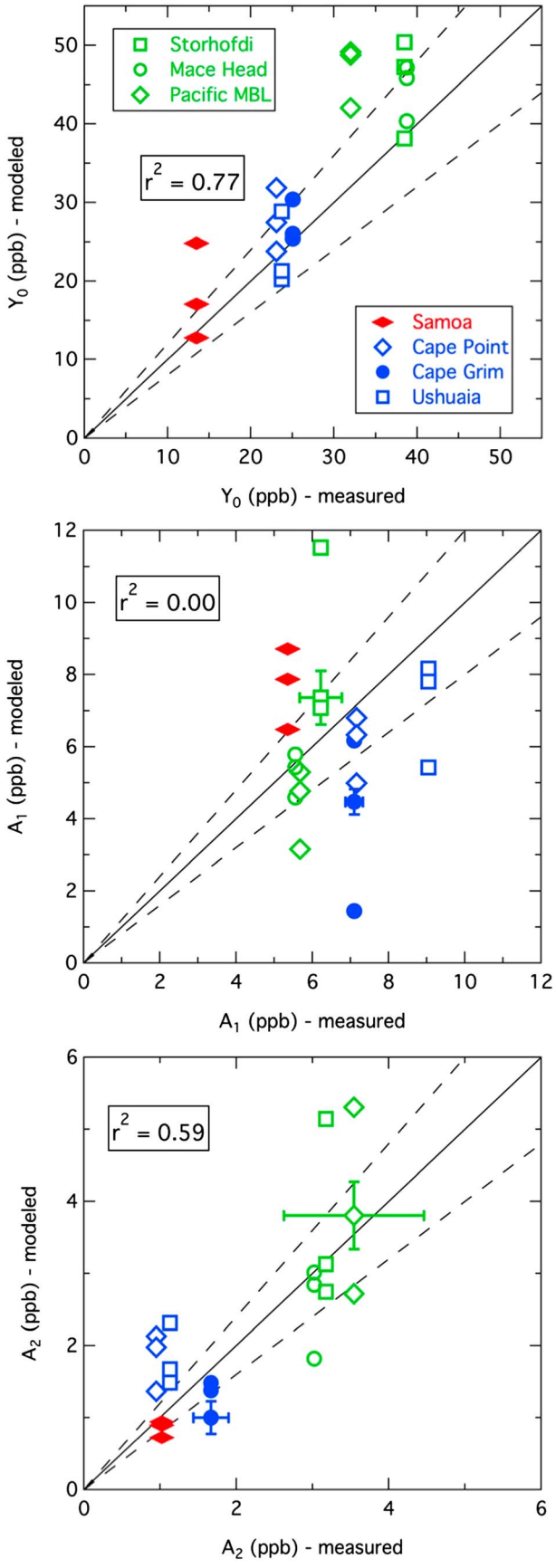

Nova Scotia, Canada) and found the seasonal cycles at all of these sites to be qualitatively consistent with those illustrated in Figures 4 and 5.

4.2. Quantitative Comparison of Seasonal Cycles Between Models and Measurements

Five parameters have been derived from the fundamental and second harmonic terms of the Fourier expansion of the measured O_3 seasonal cycles at the 11 MBL sites considered here; Table 2 gives their values with 95% confidence limits. These parameters capture nearly all of the systematic, statistically significant information regarding the seasonal cycles that can be extracted from the measurements. Thus, they provide a concise set of metrics for quantitative comparisons of model-calculated seasonal cycles with those measured. Here we provide an example comparison based on the results of the three CCMs considered here at seven sites; this comparison is illustrated in Figures 6 and 7. In these figures, example error bars are given for the parameters; the examples were chosen to display the range of precision in these determinations.

Y_0 is compared between models and measurements in the top panel of Figure 6. The r^2 value of 0.77 indicates that the models capture the systematic variation of absolute O_3 concentrations with latitude, with the highest concentrations at northern midlatitudes (where the majority of anthropogenic emissions of O_3 precursors are located), lower concentrations at southern midlatitudes, and still lower concentrations in the tropics. The models on average overestimate Y_0, most notably at the northern midlatitude sites, consistent

Figure 6. Comparison of modeled versus measured Y_0 and the amplitudes of the fundamental and second harmonic fits to seasonal cycles for MBL sites in the northern (green symbols) and southern (blue symbols) midlatitudes and the one tropical site (red symbol). Error bars show 95% confidence limits for the amplitudes from two data sets. Black lines indicate perfect agreement (solid) and agreement within ± 20% (dashed).

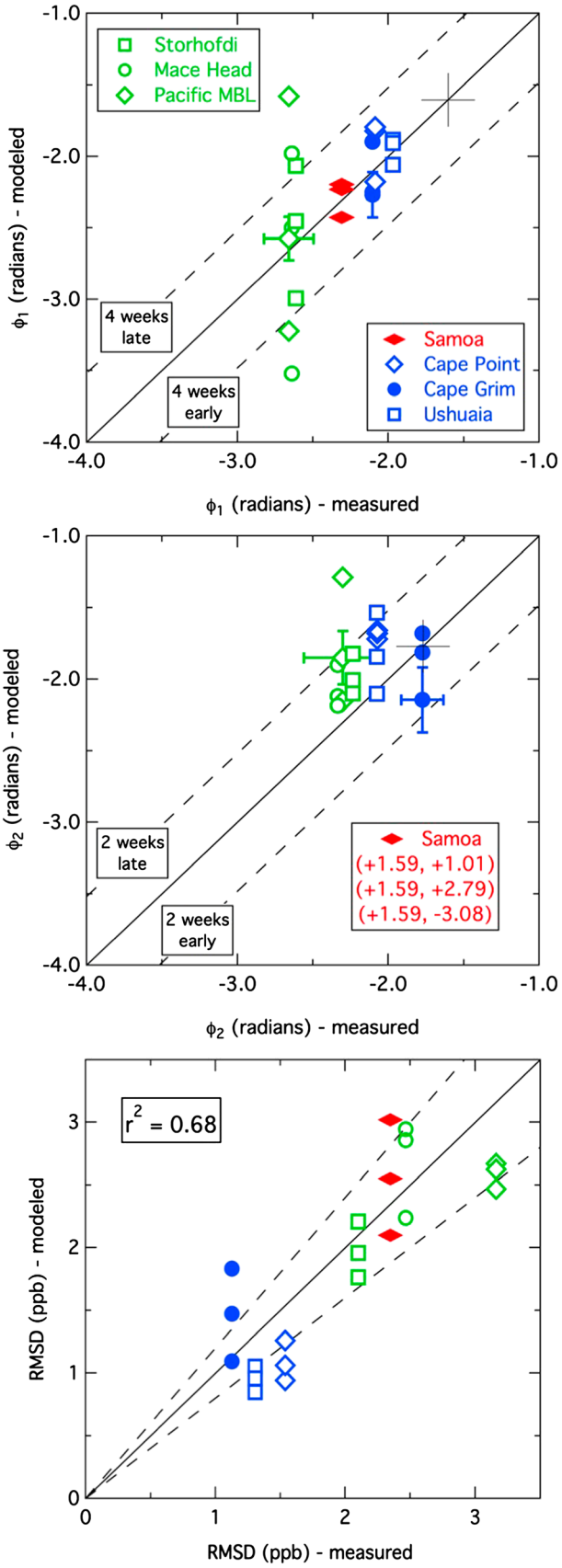

with the conclusions of *Parrish et al.* [2014], who found that absolute O_3 concentrations are generally overestimated at all sites at northern midlatitudes, particularly at the sites with the lower O_3 concentrations characteristic of the MBL. Here we see that the overestimate is much less significant in the Southern Hemisphere with most comparisons agreeing within ±20%. Two models significantly overestimate Y_0 at the one tropical site, one by nearly a factor of 2.

Compared to the fundamental, the models more accurately reproduce the second harmonic of the seasonal cycles, so this comparison is discussed before that of the fundamental. Figure 7 and Table 2 indicate that measurements find very little variability between midlatitude sites in the phase of the second harmonic, ϕ_2. Excluding Cape Grim, the ϕ_2 values at the midlatitude sites span only 0.27 rad, indicating that the maxima of the second harmonic are coincident within 8 days (ϕ_2 must span a range of 4π rad to shift the phase by an entire year), while the Cape Grim maxima are approximately 13 days earlier than the average at the other sites. The three CCMs generally reproduce ϕ_2 accurately at midlatitudes with an

Figure 7. Comparison of modeled versus measured phases of the fundamental and second harmonic fits to seasonal cycles and the root-mean-square deviation of the data points from the fits for MBL sites in the northern (green symbols) and southern (blue symbols) midlatitudes and the one tropical site (red symbol). The Northern Hemisphere ϕ_1 values are shifted by $-\pi$ to facilitate direct comparison with those from the Southern Hemisphere. The Samoa ϕ_2 values are off scale; an annotation gives those values. Error bars show 95% confidence limits for the phases from two data sets. Solid black lines indicate perfect agreement. Dashed lines indicate agreement within ±delta ϕ corresponding to (top) 4 weeks and (middle) 2 weeks in the phase, or agreement within (bottom) ±20%. The cross symbols in Figure 7 (top and middle) indicate the phase angles expected if the seasonal cycle of O_3 were of exactly opposite phase with the photolysis rate of ozone measured at Cape Grim *Wilson* [2015] (see Figure 8).

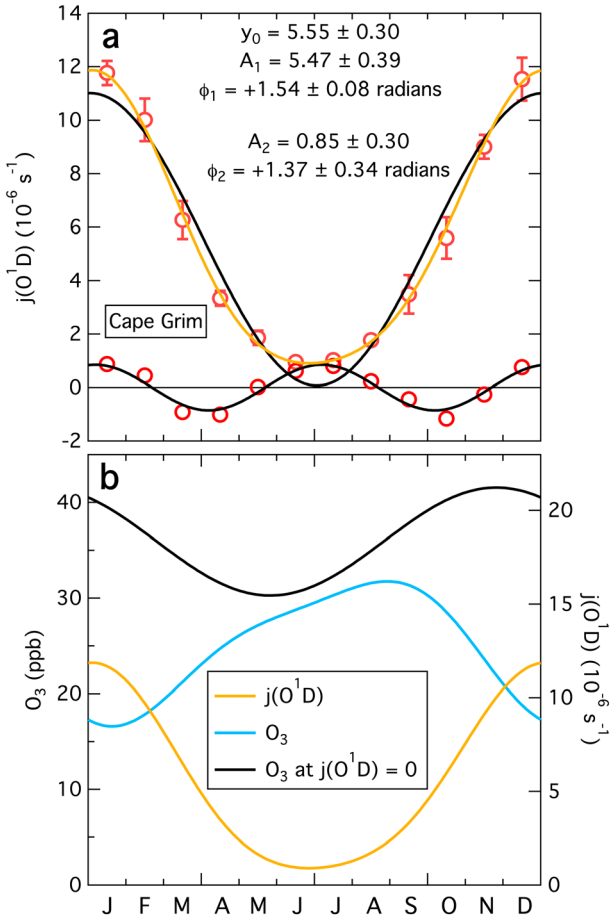

Figure 8. (a) Sine function fits to the measurements (red circles with error bars indicating standard deviation) of the monthly mean photolysis rate of O_3 ($j(O^1D)$) at Cape Grim reported by *Wilson* [2015]. The black curves give the least squares regressions to the fundamental and second harmonic terms, and the gold curve shows their sum. The data points about the *x* axis are the residuals between the measurements and the fundamental fit. The parameters of the fits with 95% confidence limits are annotated. (b) Seasonal cycle of O_3 mixing ratio expected in the MBL at Cape Grim in the absence of photolytic loss of O_3 (black curve). The blue and gold curves are reproduced from Figures 3 (top) and 6 (top), respectively. The ordinate scales are chosen so that the second harmonic amplitudes of O_3 and the photolysis rate would be equal if included in the plot.

average absolute deviation of 0.31 rad, or about 9 days, and maxima systematically late by 0.27 rad or about 8 days. An exception to this common behavior is the second harmonic observed at the two tropical sites; ϕ_2 derived for Samoa and Barbados are much different from those at midlatitudes. The three models give widely divergent phase angles (+1.01, +2.79, and −3.08 rad) for the second harmonic at Samoa; none of which agree well with the observational determination (+1.59 ± 0.41 rad), although this determination has substantial uncertainty due to the small magnitude of its amplitude (1.0 ± 0.4 ppb) and the relatively large interannual variability at this tropical site. Figure 6 shows that the models have significant skill in reproducing the variability of the second harmonic amplitude, A_2, with an r^2 value of 0.59.

Models generally reproduce the average magnitude of the fundamental, A_1, (Figure 6) over all of the sites, but none of the site-to-site variability ($r^2 = 0.00$). Examples of poor model performance include the near lack of a seasonal cycle in one model at Cape Grim and an overestimate by another model by nearly a factor of 2 at Storhofdi, Iceland. The phase of the fundamental term, ϕ_1, (Figure 7) is well reproduced in the Southern Hemisphere and at the tropical site, but model results exhibit larger variability in the Northern Hemisphere. The measurements indicate that the maximum of the fundamental term is shifted toward later in the year at northern midlatitudes by 30 to 40 days compared with the other sites. On average the models reproduce this shift, but the modeled phases are in error by up to 2 months at northern midlatitudes.

Since the models use free-running meteorology calculated by the models themselves, they cannot reproduce the time series of year-to-year variability about the average seasonal cycles that is actually observed at the sites; however, a statistical comparison is possible. Figure 7 compares the root-mean-square deviation (RMSD) of the monthly averages about the fit to the seasonal cycle calculated by the models to that observed. The models generally provide good approximations to the observed RMSD and capture the larger variability in the northern midlatitudes and tropics compared to the Southern Hemisphere sites ($r^2 = 0.68$).

4.3. Second Harmonics of $j(O^1D)$ and O_3 Seasonal Cycles

From the discussion above it is clear that the second harmonic term of the MBL O_3 seasonal cycle is a robust feature of the atmosphere, found in both the measurements and the model results at all MBL sites. To our knowledge this second harmonic has not been documented or discussed previously. It can be argued that

Table 3. Parameters of Fourier Series Fits to Measured and Modeled j(O^1D) Seasonal Cycles at Cape Grim, Tasmania, and Relationship to Respective O_3 Seasonal Cycles

	Measured	NCAR Model	GFDL Model	GISS Model
		j(O^1D) Parameters		
Y_o (10^{-6} s^{-1})	5.55 ± 0.30	5.31 ± 0.07	4.44 ± 0.03	7.22 ± 0.05
A_1 (10^{-6} s^{-1})	5.47 ± 0.39	5.44 ± 0.10	4.47 ± 0.05	5.41 ± 0.07
ϕ_1 (rad)	1.54 ± 0.08	1.54 ± 0.02	1.53 ± 0.01	1.49 ± 0.01
A_2 (10^{-6} s^{-1})	0.85 ± 0.30	0.94 ± 0.10	0.73 ± 0.05	0.62 ± 0.05
ϕ_2 (rad)	1.37 ± 0.34	1.34 ± 0.10	1.11 ± 0.06	1.21 ± 0.11
		Relationship to O_3 Seasonal Cycle		
$\Delta\phi_1$[a] (radians)	3.64 ± 0.09	3.81 ± 0.16	3.43 ± 0.05	3.74 ± 0.08
$\Delta\phi_2$[a] (rad)	3.15 ± 0.37	3.49 ± 0.25	2.93 ± 0.21	2.89 ± 0.27
sensitivity (10^6 ppb s)	2.0 ± 0.7	1.1 ± 0.3	2.0 ± 0.4	2.2 ± 0.6

[a]If the seasonal cycles of j(O^1D) and O3 were exactly of opposite phase, $\Delta\phi_1$ and $\Delta\phi_2$ would equal π radians.

it is a purely mathematical feature of the Fourier analysis; since the shape of the ozone seasonal cycle is not perfectly fit by the fundamental, higher harmonics in the Fourier spectra necessarily must contribute. However, here we present evidence for a direct physical cause: the second harmonic in the O_3 seasonal cycle results from a second harmonic in the seasonal cycle of j(O^1D).

Wilson [2015] reports j(O^1D) measurements at the Cape Grim site (Figure 8). Harmonic analysis of the measured monthly average photolysis rates gives results analogous to those for O_3 (Table 3). The fundamental and second harmonic terms as described in equation (1), and only those two terms, are statistically significant. The phase of the fundamental term of j(O^1D) (1.54 rad) is close to that of the seasonal cycle of the solar declination angle (1.76 rad) but is shifted approximately 2 weeks later in the season, possibly due to the seasonal cycle of the total O_3 column, which is at a maximum in spring and decreases through the summer, and perhaps also to an undocumented seasonal cycle in cloudiness at Cape Grim.

The seasonal cycle of O_3 mixing ratios is approximately of opposite phase compared to the measured j(O^1D) (see Table 3 and cross symbols in Figure 7); the differences in the fundamental phase between O_3 and j(O^1D) is 3.64 ± 0.09, where a difference of π radians is expected if the two cycles were exactly of opposite phase. The delay in the fundamental term of the O_3 cycle from exactly opposite phase (0.5 rad or about 1 month) is presumed to reflect the seasonal cycle of O_3 in the FT, which constitutes the source of O_3 in the MBL, as well as possible unexplored seasonal cycles in depth of the MBL, specific humidity, and the rate of entrainment into the MBL from the FT. The finite lifetime of O_3 within the MBL may also contribute to the delay; only if this lifetime is very short will the O_3 seasonal cycle directly reflect the seasonal cycle of j(O^1D).

Several lines of reasoning support the hypothesis that the second harmonic of the O_3 seasonal cycle is directly related to the photolytic loss of O_3, driven by j(O^1D). First, the close to opposite phases of the second harmonics of O_3 and j(O^1D), 3.15 ± 0.37 rad, at the midlatitude Cape Grim site, is consistent with the expected difference of π radians. Second, very similar behavior of the second harmonic of the O_3 seasonal cycle is seen at all extratropical sites. Such good agreement in phase at sites widely spaced around the globe and the excellent reproduction of the phase by the models suggest the second harmonic arises from a highly regular cyclic phenomenon that is accurately reproduced by the models; the annual cycle of actinic flux is such a phenomenon. Indeed, *Wilson* [2015] found that j(O^1D) at Cape Grim is accurately reproduced by radiation model estimates. Third, the phase behavior of the measured and modeled second harmonic of the O_3 seasonal cycle at the two tropical sites (Samoa and Barbados, Table 2) is very different from that found at the other sites. Measurements of j(O^1D) are not available from a tropical site, but the Fourier spectra of photolysis rates are expected to be very different in the tropics, since the solar zenith angle reaches a minimum twice per year, in contrast to once per year in the extratropics. This expected difference is consistent with the observed and modeled difference between the tropics and midlatitudes. Finally, as discussed in the next paragraph, the relative magnitudes of the two harmonics of O_3 and j(O^1D) at Cape Grim are consistent with a causal relationship.

If it is assumed, first, that the conceptual model described in section 4.1 can be taken as approximately correct, and second, that O_3 in the MBL responds linearly to variation in j(O^1D), then an estimate can be made of the seasonal cycle of O_3 mixing ratios in the MBL that would be present in the absence of photochemical destruction. The second harmonic of measured j(O^1D) can be considered as a perturbation of the photolytic-driven

O_3 loss rate in the MBL, resulting in a response of the MBL O_3 mixing ratio. This response is quantified by the magnitude of the second harmonic of O_3, so the ratio of A_2 derived for the O_3 mixing ratio (1.67 ± 0.23 ppb) to A_2 derived for $j(O^1D)$ ($0.85 \pm 0.30 \times 10^{-6}\ s^{-1}$) provides an estimate for the sensitivity of MBL O_3 to $j(O^1D)$ intensity ($2.0 \pm 0.7 \times 10^6$ ppb s) at Cape Grim. As illustrated in Figure 8b, this sensitivity can be used to derive an estimate (black curve) for the O_3 seasonal cycle that would exist in the MBL at Cape Grim if the loss due to photolytic processes were turned off. If nonphotolytic O_3 loss processes are negligible and if other contributions to the O_3 seasonal cycle are unimportant, then the MBL O_3 mixing ratios would track those in the FT from where the MBL O_3 is entrained. The black curve in Figure 8b is at a maximum in late austral spring, which is similar to the O_3 seasonal cycle at ~2 km altitude above a site 300 km north of Cape Grim [*Ayers et al*., 1992] and is consistent with the general understanding of the seasonal cycle of O_3 in the FT [e.g., *Monks*, 2000].

Calculations of monthly average $j(O^1D)$ at Cape Grim are available from the CCMs considered in this work. Table 3 shows that one model reproduced the five parameters derived from the measured seasonal cycle of $j(O^1D)$ within the experimental confidence limits, and the other two models accurately reproduced the phases of the fundamental and second harmonic terms but underestimated or overestimated the magnitude of $j(O^1D)$ by about 20 to 30%. All three models approximately reproduced the observed phase differences between the fundamental and second harmonic terms of the seasonal cycles of O_3 and $j(O^1D)$. Interestingly, the model that more accurately reproduced $j(O^1D)$, nevertheless underestimated the sensitivity of MBL O_3 to $j(O^1D)$ intensity by a factor of about 2, while the other two models that underestimated or overestimated the magnitude of $j(O^1D)$ closely matched this sensitivity.

4.4. Model Grid Size Considerations in Comparisons

One significant uncertainty in the comparisons discussed in section 4.2 arises from the spatial mismatch between the measurements made at a single point and the model calculations that are effectively an average over a single grid cell in the model. The grid cells for the three models are all approximately 2° latitude by 2.5° longitude. Thus, for the coastal sites considered in this work, the model grid cell likely contains both marine and continental areas. This combination may bias the model-measurement comparisons, since the measurements are assumed, and in some cases selected, to represent marine conditions. Here we investigate this issue by comparing measurements with model results for the grid cell containing the coastal measurement site and for a grid cell at a more remote, offshore marine location. We consider four cases; the first three compare model results from measurement sites on the coasts of the eastern Atlantic and the eastern Pacific (section 4.4.1), while the fourth compares model results from measurements on the western coast of Japan (section 4.4.2). The fourth comparison is of particular interest since the offshore marine location is in the middle of the Sea of Japan, which is downwind of the East Asian continent, and thus more heavily influenced by upwind continental emissions than are the Atlantic and Pacific sites. In each case, the seasonal cycle derived from measurements at the coastal site is assumed to represent the seasonal cycle at the marine location. The four measurement sites considered in these comparisons are the four northern midlatitude sites in closest proximity to heavily populated and industrialized areas, and thus present the greatest possibility of confounding influences.

4.4.1. Comparisons of Upwind Locations With Coastal Atlantic and Pacific Sites

Measurement results from two Atlantic sites, Mace Head and Storhofdi, will be compared with model calculations at the grid point corresponding to each site and at a single point that is ~440 km west of Mace Head and ~1200 km south-southeast of Storhofdi. Mace Head and Storhofdi are approximately 1300 km apart. The validity of comparing measurements at these two coastal sites with model calculations at a single point in the marine environment relatively far removed from either site depends upon the uniformity of the seasonal cycle of O_3 over this entire region. The seasonal cycles derived from the measurements at Mace Head and Storhofdi (Figure 4) are indeed very similar, and none of the five parameters derived from the Fourier series fits (Table 2) is statistically different between the two sites. This similarity supports the validity of this comparison. The Pacific comparison is between the experimental results from the Pacific MBL sites with model calculations at Trinidad Head and at a point ~330 km west (41.05°N latitude 128°W longitude).

Figure 9 contrasts the comparisons discussed in the previous section (Figures 6 and 7) with those for these offshore, marine grid cells. The primary conclusion from Figure 9 is that there are no major differences in the comparison of measurements with model results sampled at a grid cell directly over the site or at an exclusively marine grid cell. The measurement sites selected for comparison with model results in this paper

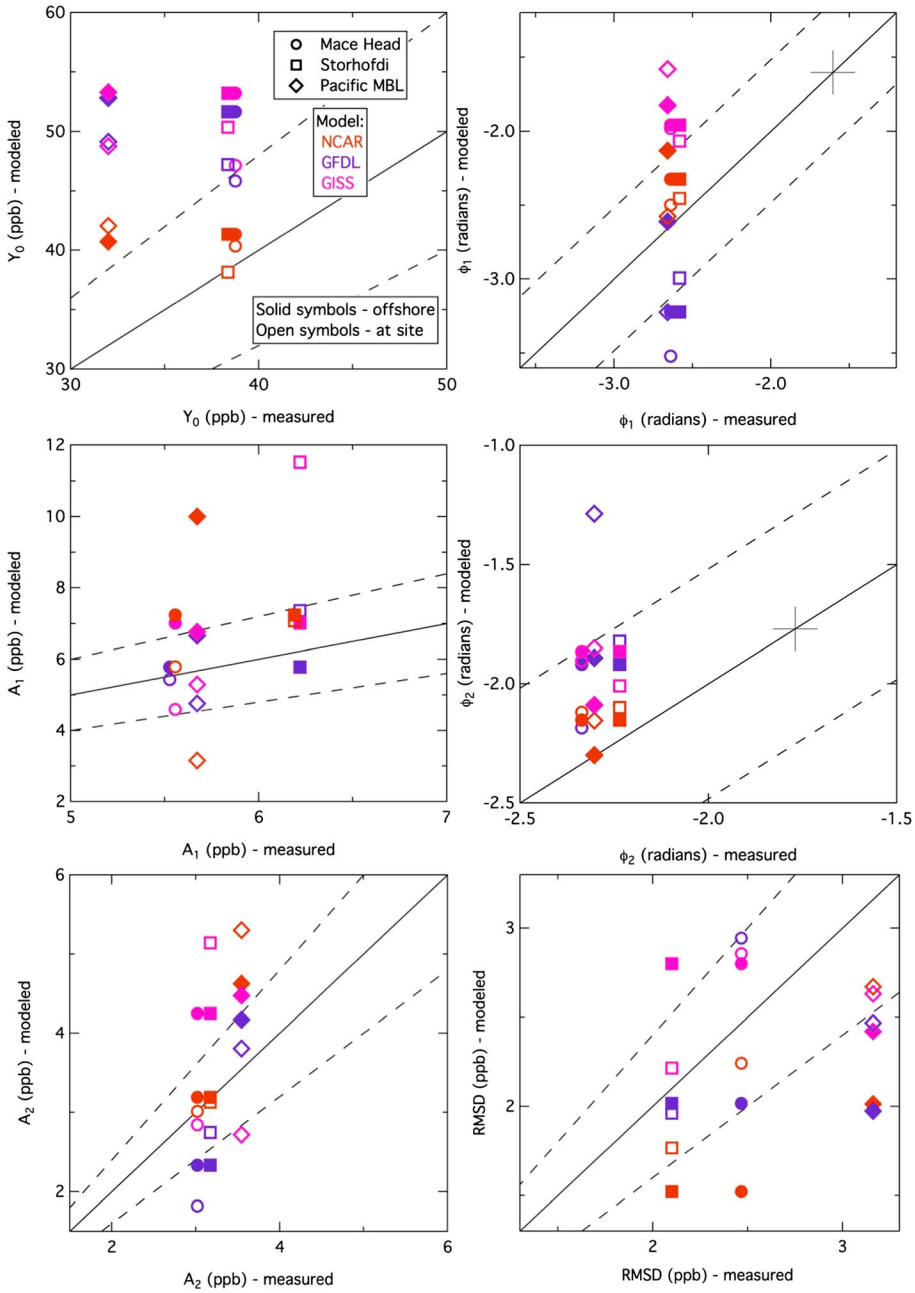

Figure 9. Comparison of modeled versus measured seasonal cycle parameters for three northern midlatitude sites based on model grids including the sites (open symbols) and on model grids 330 km west of Trinidad Head and 440 km west of Mace Head. Figures are in the same format as Figures 7 and 8, except that the axes have been expanded. Some points are offset by an inconsequential amount to allow all symbols to be discerned.

were chosen to represent baseline conditions as closely as possible. The relatively small differences in the comparisons indicate that the selected measurements do indeed represent baseline conditions characteristic of large regions, so that comparisons between measurement and model results are relatively insensitive to their exact colocation.

The offsets between the model and measured annual average, Y_0, are nearly always significantly greater in the purely marine comparison (Figure 9). This positive model offset, which averages 26% high (range of 1% low to and 53% high) for these sites in the original comparison, increases to an average of 35% high (range of 7% to 67% high) in the marine comparison, suggesting that the comparisons are better when

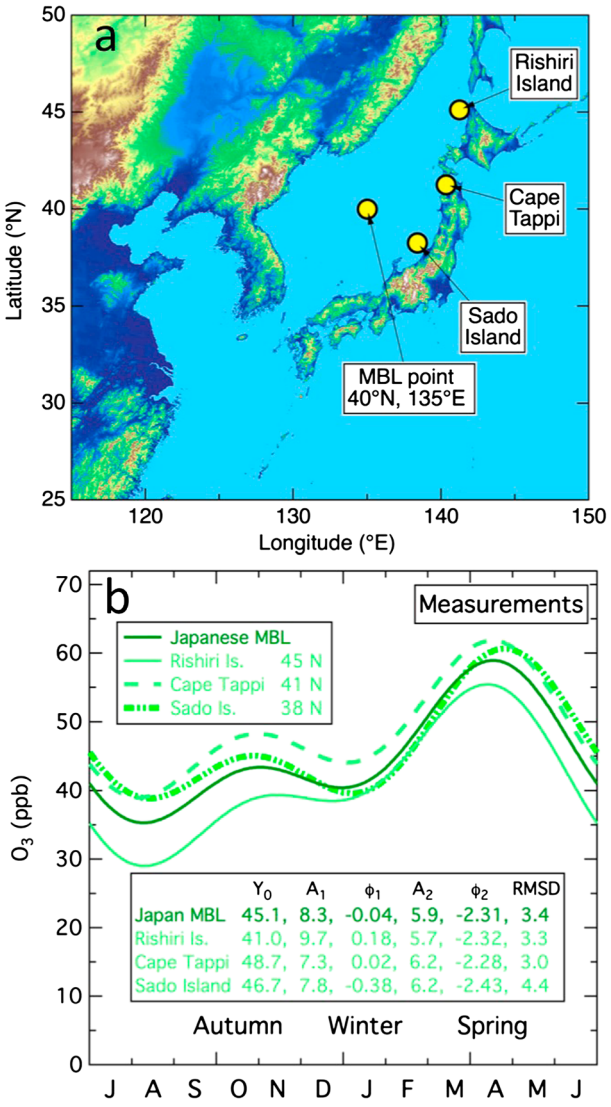

Figure 10. (a) Map of Japanese MBL sites with the offshore location of model results indicated in the Sea of Japan. (b) Comparison of O_3 seasonal cycles derived from measurements at the three MBL sites with that derived from the combined data sets. The parameters of the Fourier series fits that define the seasonal cycles are annotated in the graph. Note the order of seasons on the abscissa; they are set to be consistent with other figures.

the model combines continental influences with the marine environment, i.e., when model results are sampled directly over the site. Section 4.4 further discusses the cause of this model overestimate, and why the overestimates are particularly large in the marine environment.

The model reproduction of the fundamental term of the seasonal cycle is somewhat improved in the marine grid cells. The largest measurement-model discrepancies in the phase angle, ϕ_1, in Figure 7 are from the sites subject to this comparison, and Figure 9 indicates that these discrepancies are improved by sampling the marine grid cells. The range of discrepancies decreased from −0.88 to +1.08 rad in the original comparison to −0.61 to + 0.84 rad in the marine comparison, with the average absolute discrepancy remaining nearly constant at 0.50 rad, corresponding to an average absolute offset of about 29 days. The model estimated magnitude of the fundamental, A_1, is also improved in some respects; in the original comparison it averaged 4% high but, the estimates ranged from 44% low to 85% high, while in the marine comparison it averaged 22% high, but the range of the estimates decreased (7% low to 76% high).

The model reproduction of the second harmonic term of the seasonal cycle is improved in the marine grid cells. The phase angle, ϕ_2, is better reproduced with the results from all nine models within 2 weeks of the measured phase, an average phase discrepancy of 0.28 rad (i.e., 8 days), and the largest discrepancy in the initial phase comparison greatly improved. The estimates of the magnitude of the second harmonic, A_2, improved as well; the range of the model estimates decreased from 40% low to 62% high in the original comparison to 27% low to 41% high in the marine comparison, while the average continued to indicate good agreement (4% high in the original comparison and 12% high in the offshore comparison).

4.4.2. Comparisons of Onshore and Offshore Sites in the Sea of Japan

The Sea of Japan is the marine region directly east of northeast China and the Korean Peninsula and west of Japan (Figure 10a). The East Asian monsoon generally controls atmospheric transport in this region with northwesterly flow dominating during most of the year (September through June). These northwest winds bring continental air with pollution outflow from northeast China and the Korean Peninsula into the Sea of Japan region [*Tanimoto et al.*, 2005]. The winds shift to southerly during summer, bringing marine air with possible pollution outflow from Japan. The growing emissions of O_3 precursors in East Asia enhance the importance of this region to the O_3 budget of the troposphere. However, the close proximity of the

Table 4. Parameters of Fourier Series Fits to O_3 Seasonal Cycles for MBL Surface Sites in the Sea of Japan

Location	Y_o (ppb)	A_1 (ppb)	ϕ_1 (rad)	A_2 (ppb)	ϕ_2 (rad)	RMSD (ppb)
			Measurements			
Sado Island	46.7 ± 1.6	7.8 ± 2.3	−0.38 ± 0.30	6.2 ± 2.3	−2.43 ± 0.37	4.4
Cape Tappi	48.7 ± 1.1	7.3 ± 1.6	0.02 ± 0.21	6.2 ± 1.6	−2.28 ± 0.25	3.0
Rishiri Island	41.0 ± 1.1	9.7 ± 1.6	0.18 ± 0.16	5.7 ± 1.6	−2.32 ± 0.28	3.3
Japanese MBL	45.1 ± 1.4	8.3 ± 2.0	−0.04 ± 0.24	5.9 ± 2.0	−2.31 ± 0.34	3.4
			Model Results			
NCAR Sado Island	46.1 ± 0.5	1.3 ± 0.7	0.22 ± 0.56	3.3 ± 0.7	−1.80 ± 0.22	3.1
NCAR 40°N, 135°E	45.2 ± 0.4	2.4 ± 0.6	−0.82 ± 0.24	2.5 ± 0.6	−1.74 ± 0.23	2.5
GFDL Sado Island	50.8 ± 0.4	6.1 ± 0.6	−0.04 ± 0.10	3.4 ± 0.6	−1.42 ± 0.18	1.9
GFDL 40°N, 135°E	58.9 ± 0.5	7.4 ± 0.8	−0.66 ± 0.10	4.0 ± 0.8	−2.10 ± 0.19	3.0
GISS Sado Island	61.2 ± 0.6	1.5 ± 0.8	−1.75 ± 0.58	1.4 ± 0.8	−0.16 ± 0.58	3.6
GISS 40°N, 135°E	62.0 ± 0.6	3.1 ± 0.8	−1.78 ± 0.27	2.2 ± 0.8	0.44 ± 0.37	3.8

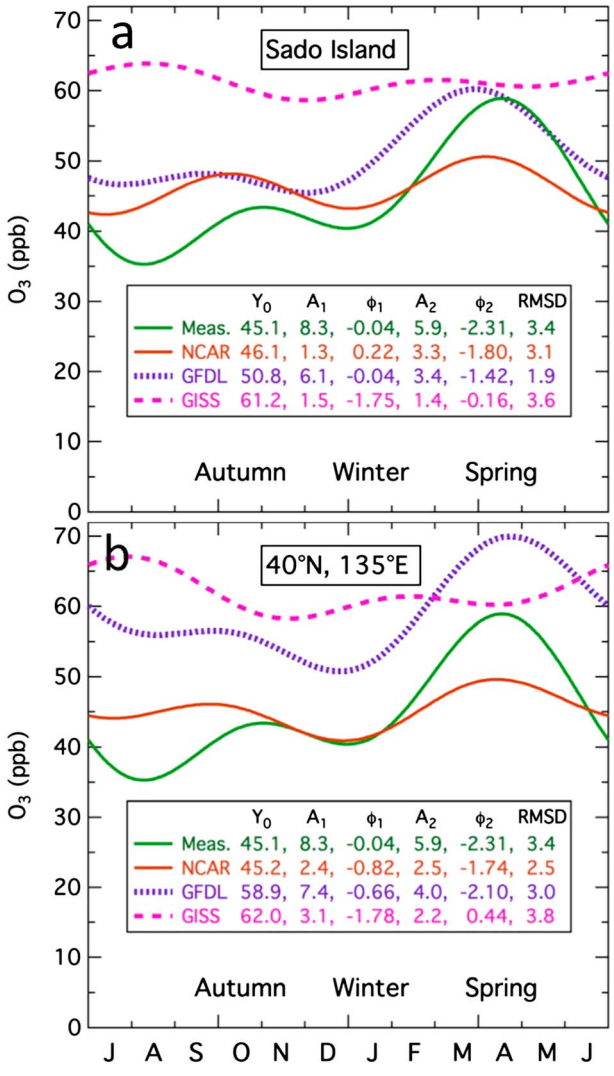

Figure 11. Comparison of O_3 seasonal cycles derived from measurements and model results at (a) Sado Island and (b) the Sea of Japan site at 40°N, 135°E. In each graph the measurement results are for the combined Japanese MBL data sets. The parameters of the Fourier series fits that define the seasonal cycles are annotated in the graphs. Note the order of seasons on the abscissa; they are set to be consistent with other figures.

continental emission sources to this relatively small marine region may present a challenge to modeling by relatively coarse grid CCMs. Here we compare results from measurements at three relatively isolated MBL sites on the west coast of Japan with model results at one of those sites (Sado Island) and at a marine point (40°N latitude and 135°E longitude) lying about 350 km offshore (see Figure 10a).

Measurements from the MBL sites on the west coast of Japan (Figure 10a) provide a characterization of the seasonal O_3 cycle in this marine region. These three sites, which constitute the Japanese MBL data set, span the region from 38.3° to 45.1°N latitude and 138.4° to 141.2°E longitude, yet the O_3 seasonal cycles separately derived from the measurements are similar at all three sites. The relatively small differences between the sites in Figure 10b are consistent with the discussion of *Tanimoto et al.* [2005]. The five parameters of the Fourier series fits are given both in the figure annotation and with their 95% confidence limits in Table 4. Statistically significant differences in the parameters between sites are generally limited to Y_0. The seasonal cycle derived from the combined data sets (darker green line in Figure 10b, also included in Figures 5 and 11) is consistent with those from each of the separate sites and is used for comparison with the model results. The consistency of the seasonal cycles in Figure 10b derived from measurements

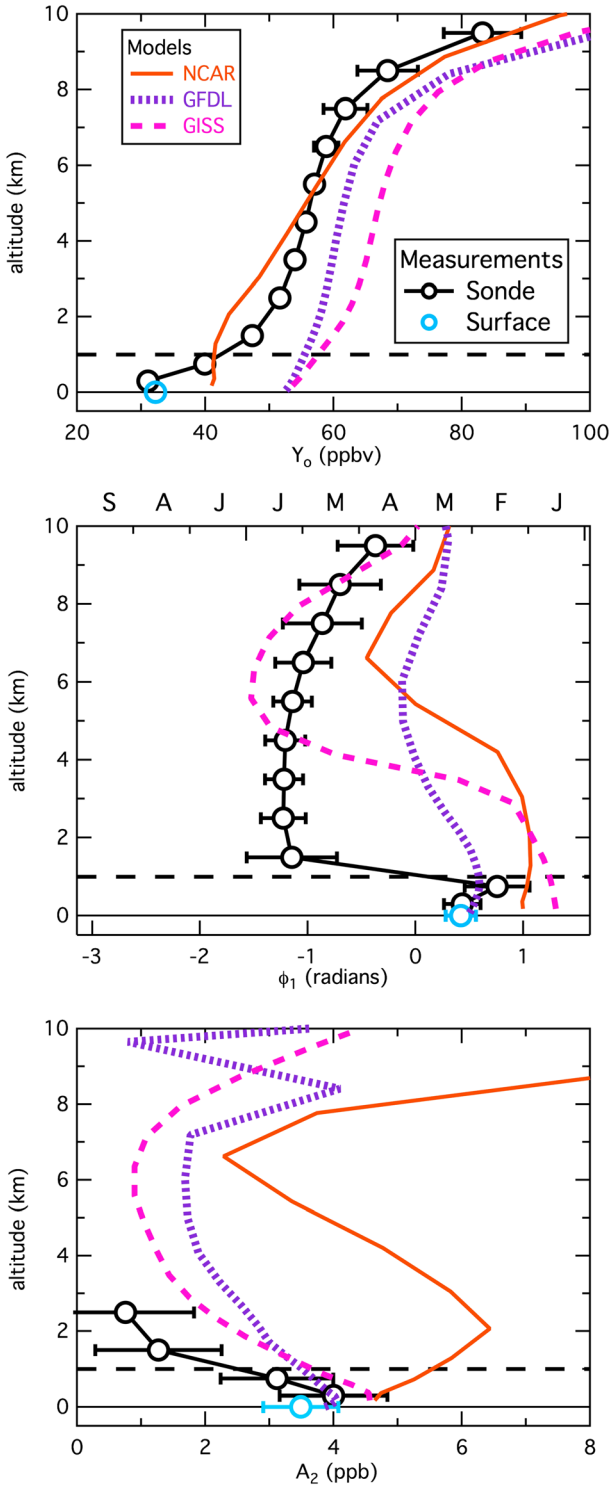

Figure 12. Comparison of modeled versus measured altitude dependence of the O_3 seasonal cycle. Three of the Fourier series fit parameters for the ozonesonde data in 0.5 km altitude increments above Trinidad Head are shown. For the models, seasonal cycles are calculated at each model layer at a point 330 km west of Trinidad Head to avoid continental influences. The blue symbols indicate the corresponding parameters derived from the surface measurements. The black dashed line indicates the approximate top of the marine boundary layer.

at three sites that span about 800 km of the western Japanese coast suggests that these measurements accurately characterize the marine O_3 seasonal cycle, which evidently varies little over this region.

Comparisons of the model results with the measurements at the coastal sites (Figure 11a) and at the offshore marine location (Figure 11b) indicate that the models have some difficulties reproducing the observed O_3 seasonal cycle. The models generally underestimate the magnitude of the fundamental amplitude, two by a factor of about 6 at Sado Island yielding quite flat seasonal cycles. The one model that closely captures the fundamental term finds a large phase difference in the second harmonic, which gives an overall seasonal cycle that peaks about 1 month early. Comparison between the measurements and the model results at the offshore point is not markedly improved.

4.5. Altitude Dependence of Comparisons

Ozonesondes launched since 1997 at Trinidad Head allow the model-measurement comparison of seasonal cycles to be extended to above the MBL at this one site. We compare with the model results from the point 330 km west of Trinidad Head to minimize continental influence. Figure 12 illustrates comparisons for three of the five parameters derived from the harmonic analysis of the seasonal cycles through the lower 10 km of the troposphere. The measurements show strong gradients between the MBL and the lower FT for all three parameters, gradients that the models only poorly reproduce.

The altitude dependence of the measured seasonal cycle in Figure 12 is consistent with the conceptual model discussed in section 4.1. Within the MBL the ozone budget is dominated by photochemical destruction balanced by entrainment of ozone from the FT. Thus, the annual average O_3 (Y_0) is lowest near the surface and

significantly larger above the MBL. The vertical gradient is smaller through the midtroposphere and increases in the upper troposphere where the stratospheric influence dominates. The phase of the fundamental term (ϕ_1) gives a late winter (February and March) seasonal maximum and a late summer minimum in the MBL, consistent with the seasonal cycle of the rate of photochemical removal. The seasonal maximum shifts to June immediately above the MBL consistent with a smaller influence of photochemical destruction and the dominance of photochemical production of O_3 in the lower FT. In the upper troposphere the seasonal maximum shifts to spring when the stratospheric influence maximizes. We have attributed the second harmonic of the O_3 seasonal cycle to the second harmonic of the photolysis rate of O_3, which drives the photochemical destruction in the MBL; consistent with this attribution the magnitude of the second harmonic derived from the measurements decreases rapidly above the MBL.

The results from all three models do not fit this hypothetical picture. The gradients between the MBL and the lower FT of all three parameters in Figure 12 are not nearly as strong as found in the measurements. The model results do not show the strong reduction of O_3 within the MBL; there is no strong shift in O_3 seasonal cycle immediately above MBL, and the second harmonic has significant magnitudes through the troposphere. These model-measurement differences are primarily attributed to inadequate treatment of the MBL structure and dynamics within the three CCMs examined here. The MBL is usually capped by a strong temperature inversion, which is in part related to stratiform cloud processes; global models do not reproduce these inversions well [*Soden and Vecchi*, 2011; *Qu et al*., 2014]. Inadequate treatment of the capping inversion may allow more rapid entrainment of O_3 into the MBL. As a result, modeled O_3 depletion is not great enough to reproduce the strong vertical gradient of O_3 from the lower FT (Figure 12) and contributes to the model overestimate of annual average O_3. An enhanced influence of halogen chemistry within the MBL [*von Glasow et al*., 2002; *Saiz-Lopez et al*., 2012] may also contribute to low O_3 concentrations observed within the MBL, and the chemical schemes of the CCMs considered here do not include this chemistry.

5. Summary and Conclusions

A quantitative description of the seasonal O_3 cycle in the MBL has been developed based upon harmonic analysis. In addition to the fundamental term that describes the majority of the seasonal variation, it is found that a second harmonic term (i.e., two sine cycles per year) is a ubiquitous feature of MBL sites throughout the world. This second harmonic term is found both in the measurements and model results at all MBL sites examined but is absent in sonde measurements in the FT. Five parameters are necessary to define the seasonal cycle in either the measurements or the model results, and these parameters provide quantitative metrics with which to compare the model results to the measurement data. The parameters derived from the measurements are given in Tables 2–4; they can be utilized to evaluate results from other model simulations of tropospheric O_3 in the MBL.

The measurements and modeling agree that O_3 in the MBL maximizes in late winter to early spring in both hemispheres, with the Northern Hemisphere exhibiting higher annual average concentrations than the Southern Hemisphere; the tropical sites have significantly lower concentrations than the midlatitudes. We attribute the primary cause of this seasonal cycle to photochemical destruction of O_3 within the MBL, balanced by entrainment of higher concentrations of O_3 from the FT. A second harmonic term in the photolysis rate of O_3, which was measured at the Cape Grim site, is believed to lead to the second harmonic term observed at all of the MBL sites.

The three models considered each capture many characteristics of the measured O_3 seasonal cycles in the MBL at northern and southern midlatitudes and at one tropical site, but there are specific biases of the model calculations identified by the quantitative comparison metrics. Most notably, the three CCMs examined here overestimate MBL O_3 in the Northern Hemisphere by about 20–65%, an overestimate identified earlier [*Parrish et al*., 2014]. There are also inaccuracies in reproducing the fundamental term of the seasonal cycle. Overall, the average magnitude is reproduced well, but the models do not capture observed site-to-site variability, with both high and low errors throughout the sites. There are errors in the calculated phases at northern midlatitude sites, but the seasonal peak of the fundamental term is reproduced within < 4 weeks at other sites. Interestingly, the second harmonic term is generally more accurately reproduced by the models than is the fundamental term. This is consistent with the hypothesis that the photolysis rate of O_3 is the dominant cause of the second harmonic term, since it is expected that the models can accurately calculate the solar

actinic irradiance field but may have more difficulties reproducing the many other processes that contribute to seasonal variations of tropospheric O_3.

For data sets from four coastal sites, the seasonal cycle derived from measurements is also compared with model results from a nearby offshore grid cell that is expected to represent a pure marine environment without inclusion of a segment of land mass. Only marginal improvements were found by shifting the model-measurement comparisons from the model grid directly over the site to the exclusively marine grid cell. Models demonstrate particular difficulty in simulating the O_3 seasonal cycle in the Sea of Japan region, where atmospheric transport is dominated by the East Asian monsoon that brings pollution outflow from the East Asian continent through much of the year, but marine air in summer.

Analysis of data from sondes launched at the Trinidad Head site allows comparisons through the depth of the troposphere at this one location. In the lower FT the model-measurement agreement is not nearly as good as in the MBL with strong vertical gradients in the O_3 seasonal cycle poorly reproduced. This lack of agreement above the MBL is interpreted as indicating that the models do not adequately reproduce the isolation of the MBL. As a result the models cannot properly separate O_3 destruction in the MBL from O_3 production in the lower FT. Missing halogen chemistry in the models could also influence the model-observation comparison over the MBL where oceanic halogen emissions have been shown to provide an additional sink of O_3. Detailed analysis of simulated O_3 budget terms (e.g., photochemical loss and production, deposition, and transport) within the MBL through model comparison to data sets with more comprehensive composition, and meteorological measurements could help isolate the reasons for the model biases presented here.

Acknowledgments

The CESM project (which includes the CAM-chem model) is supported by the National Science Foundation and the Office of Science (BER) of the U.S. Department of Energy. NCAR is operated by the University Corporation of Atmospheric Research under sponsorship of the National Science Foundation. The authors are grateful to P.G. Simmonds and T.G Spain for providing the Mace Head data and to A.J. Manning for sorting the Mace Head data into baseline and nonbaseline observations. D. Parrish acknowledges support from NOAA's Climate Base Funds and the Atmospheric Chemistry and Climate Program. All of the observational data and model results are archived by the authors. Sources for observational data: Cape Grim, Australia-I. Galbally (Ian.Galbally@csiro.au); Mace Head-D. Derwent (r.derwent@btinternet.com); Storhofdi, Iceland, Trinidad Head, U.S., Samoa, Arrival Heights, Antarctica, Ragged Point, Barbados, and Tudor Hill, Bermuda-NOAA/GMD data archive (http://www.esrl.noaa.gov/gmd/dv/ftpdata.html); Pacific MBL-D. Parrish (david.d.parrish@noaa.gov); Japanese MBL-H. Tanimoto (tanimoto@nies.go.jp); Ushuaia, Argentina-M. Cuperio (mcupeiro@smn.gov.ar); and Cape Point, South Africa-C. Labuschagne (casper.labuschagne@weathersa.co.za). Sources for model results: CAM-chem-J.-F. Lamarque (lamar@ucar.edu); GFDL-CM3 - V. Naik (vaishali.naik@noaa.gov) and GISS-E2-R-D. Shindell (drew.shindell@duke.edu).

References

Ayers, G. P., S. A. Penkett, R. W. Gillet, B. Bandy, I. E. Galbally, C. P. Meyer, C. M. Elsworth, S. T. Bentley, and B. W. Forgan (1992), Evidence for photochemical control of ozone concentrations in unpolluted marine air, *Nature*, *360*, 446–449.

Brown-Steiner, B., P. G. Hess, and M. Lin (2015), On the capabilities and limitations of GCCM simulations of summertime regional air quality: A diagnostic analysis of ozone and temperature simulations in the US using CESM CAM-Chem, *Atmos. Environ.*, *101*, 134–148.

Cooper, O. R., et al. (2014), Global distribution and trends of tropospheric ozone: An observation-based review, *Elem. Sci. Anthropocene*, *2*, doi:10.12952/journal.elementa.000029.

Cooper, O. R., A. O. Langford, D. D. Parrish, and D. W. Fahey (2015), Challenges of a lowered U.S. ozone standard, *Science*, *348*(6239), 1096–1097, doi:10.1126/science.aaa5748.

Donner, L. J., et al. (2011), The dynamical core, physical parameterizations, and basic simulation characteristics of the atmospheric component of the GFDL global coupled model CM3, *J. Clim.*, *24*, 3,484–3,519, doi:10.1175/2011JCLI3955.

Eyring, V., et al. (2013), Long-term ozone changes and associated climate impacts in CMIP5 simulations, *J. Geophys. Res. Atmos.*, *118*, 5029–5060, doi:10.1002/jgrd.50316.

Fabian, P., and P. G. Pruchniewicz (1977), Meridional distribution of ozone in the troposphere and its seasonal variations, *J. Geophys. Res.*, *82*, 2063–2073, doi:10.1029/JC082i015p02063.

Fiore, A. M., J. T. Oberman, M. Y. Lin, L. Zhang, O. E. Clifton, D. J. Jacob, V. Naik, L. W. Horowitz, J. P. Pinto, and G. P. Milly (2014), Estimating North American background ozone in U.S. surface air with two independent global models: Variability, uncertainties, and recommendations, *Atmos. Environ.*, *96*, 284–300.

Griffies, S. M., et al. (2011), The GFDL CM3 coupled climate model: characteristics of the ocean and sea ice simulations, *J. Clim.*, *24*, 3520–3544, doi:10.1175/2011JCLI3964.1.

Lamarque, J.-F., et al. (2010), Historical (1850–2000) gridded anthropogenic and biomass burning emissions of reactive gases and aerosols: Methodology and application, *Atmos. Chem. Phys.*, *10*, 7017–7039, doi:10.5194/acp-10-7017-2010.

Lamarque, J. F., et al. (2012), CAM-chem: Description and evaluation of interactive atmospheric chemistry in the Community Earth System Model, *Geosci. Model. Dev.*, *5*, 369–411.

Lamarque, J.-F., et al. (2013), The Atmospheric Chemistry and Climate Model Intercomparison Project (ACCMIP): Overview and description of models, simulations and climate diagnostics, *Geosci. Model Dev.*, *6*, 179–206, doi:10.5194/gmd-6-179-2013.

Leith, C. E. (1973), The standard error of time-averaged estimates of climatic means, *J. Appl. Meteorol.*, *12*, 1066–1069.

Levy, H., II (1971), Normal atmosphere: Large radical and formaldehyde concentrations predicted, *Science*, *173*, 141–143.

Monks, P. S. (2000), A review of the observations and origins of the spring ozone maximum, *Atmos. Environ.*, *34*, 3545–3561.

Oltmans, S. J., and H. Levy II (1992), Seasonal cycle of surface ozone over the western North Atlantic, *Nature*, *358*, 392–394.

Oltmans, S. J., and H. Levy II (1994), Surface ozone measurements from a global network, *Atmos. Environ.*, *28*, 9–24.

Oltmans, S. J., R. C. Schnell, P. J. Sheridan, R. E. Peterson, S.-M. Li, J. W. Winchester, P. P. Tans, W. T. Sturges, J. D. Kahl, and L. A. Barrie (1989), Seasonal surface ozone and filterable bromine relationship in the high Arctic, *Atmos. Environ.*, *23*, 2431–2441.

Parrish, D. D., D. B. Millet, and A. H. Goldstein (2009), Increasing ozone in marine boundary layer inflow at the west coasts of North America and Europe, *Atmos. Chem. Phys.*, *9*, 1303–1323, doi:10.5194/acp-9-1303-2009.

Parrish, D. D., et al. (2013), Lower tropospheric ozone at northern midlatitudes: Changing seasonal cycle, *Geophys. Res. Lett.*, *40*, 1631–1636, doi:10.1002/grl.50303.

Parrish, D. D., et al. (2014), Long-term changes in lower tropospheric baseline ozone concentrations: Comparing chemistry-climate models and observations at northern midlatitudes, *J. Geophys. Res. Atmos.*, *119*, 5736–5719, doi:10.1002/2013JD021435.

Qu, X., A. Hall, S. A. Klein, and P. M. Caldwell (2014), On the spread of changes in marine low cloud cover in climate model simulations of the 21st century, *Clim. Dyn.*, *42*, 2603–2626.

Royal Society (2008), *Ground-Level Ozone in the 21st Century: Future Trends, Impacts and Policy Implications, RS Policy Document 15/08*, R. Soc., London.

Saiz-Lopez, A., et al. (2012), Estimating the climate significance of halogen-driven ozone loss in the tropical marine troposphere, *Atmos. Chem. Phys.*, *12*, 3939–3949, doi:10.5194/acp-12-3939-20122012.

Schnell, J. L., et al. (2015), Use of North American and European air quality networks to evaluate global chemistry-climate modeling of surface ozone, *Atmos. Chem. Phys. Discuss.*, *15*, 11,369–11,407, doi:10.5194/acpd-15-11369-2015.

Shindell, D. T., et al. (2013), Interactive ozone and methane chemistry in GISS-E2 historical and future climate simulations, *Atmos. Chem. Phys.*, *13*, 2653–2689.

Soden, B. J., and G. A. Vecchi (2011), The vertical distribution of cloud feedback in coupled ocean–atmosphere models, *Geophys. Res. Lett.*, *38*, L12704, doi:10.1029/2011GL047632.

Stevenson, D. S., et al. (2013), Tropospheric ozone changes, radiative forcing and attribution to emissions in the Atmospheric Chemistry and Climate Model Intercomparison Project (ACCMIP), *Atmos. Chem. Phys.*, *13*, 3063–3085, doi:10.5194/acp-13-3063-2013.

Tanimoto, H., Y. Sawa, H. Matsueda, I. Uno, T. Ohara, K. Yamaji, J. Kurokawa, and S. Yonemura (2005), Significant latitudinal gradient in the surface ozone spring maximum over East Asia, *Geophys. Res. Lett.*, *32*, L21805, doi:10.1029/2005GL023514.

von Glasow, R., R. Sander, A. Bott, and P. J. Crutzen (2002), Modeling halogen chemistry in the marine boundary layer 1. Cloud-free MBL, *J. Geophys. Res.*, *107*(D17), 4341, doi:10.1029/2001JD000942.

Wilson, S. R. (2015), Characterisation of $J(O^1D)$ at Cape Grim 2000–2005, *Atmos. Chem. Phys.*, *15*, 7337–7349, doi:10.5194/acp-15-7337-2015.

Zhang, L., D. J. Jacob, X. Yue, N. V. Downey, D. A. Wood, and D. Blewitt (2014), Sources contributing to background surface ozone in the US Intermountain West, *Atmos. Chem. Phys.*, *14*, 5295–5309, doi:10.5194/acp-14-5295-2014.